Muller Matthew (Orcid ID: 0000-0002-3835-4096)
Micheli Leonardo (Orcid ID: 0000-0001-7986-7560)
Solas Alvaro F (Orcid ID: 0000-0003-4650-9470)
Alghamdi Yusif (Orcid ID: 0000-0003-0387-5788)
Fernández Eduardo (Orcid ID: 0000-0001-7934-9755)

AN IN-DEPTH FIELD VALIDATION OF "DUSST":

A NOVEL LOW-MAINTENANCE SOILING MEASUREMENT DEVICE

Matthew Muller[1], Leonardo Micheli[2], Alvaro F. Solas[2], Michael, Gostein[3], Justin Robinson[4], Kenny Morely[4], Michael Dooraghi[4], Yusif A. Alghamdi[5], Zeyad A. Almutairi[5], Florencia Almonacid[2], Eduardo F. Fernandez[2],

[1] National Renewable Energy Laboratory, Golden, Colorado, United States

[2] Advances in PV technology Research Group (AdPVTech), University of Jaen, Jaen, Spain

[3]Atonometrics Inc., Austin, Texas

[4] GroundWork Renewables Inc., Logan, Utah

[5] Sustainable Energy Technologies Center King Saud University, Riyadh, Saudi Arabia

Abstract: This study presents indoor and field validation results for two versions of the "DUSST" optical soiling sensor, intended to be a low-cost and low-maintenance device for measuring photovoltaic soiling losses. Indoor testing covers irradiance calibration and temperature dependencies which are necessary to achieve high accuracy, low uncertainty field measurements. Field testing includes an array of different environments including: Saudi Arabia, California, Utah, and Colorado. DUSST versions include a configuration with a 530 nm LED (discussed in previous work) and a unit with 7 white LEDS and a polycarbonate collimating optic. The new design increases light intensity fivefold and demonstrates a single linear calibration coefficient is effective to measure soiling losses as high as 75%. Field data from Utah and California demonstrate that daily soiling loss measurements and soiling rate calculations closely match both reference cell and full-size module measurements of soiling losses and soiling rates. Corrective methods employed on the Utah DUSST sensor suggest that it is possible to achieve measurement errors as low as ±0.1% at two standard deviations. Field data from both Colorado and Saudi Arabia demonstrate that LED lens soiling can occur and that further design optimizations are needed. The lesson learned from all the field deployment locations suggest directions for future design improvements.

This is the author manuscript accepted for publication and has undergone full peer review but has not been through the copyediting, typesetting, pagination and proofreading process, which may lead to differences between this version and the Version of Record. Please cite this article as doi: 10.1002/pip.3415

Keywords: Soiling; Photovoltaics; Sensor; Thermal characterization; Field Testing

1. Introduction

In the past decade cumulative photovoltaic (PV) installations have grown from less than 40 GW in 2010 to 586 GW at the beginning of 2020 [1]. In line with rapid growth, PV has matured from a technology that was being installed due to tax credits or financial incentives to now being one of the lowest cost energy choices. Large installations, on a scale of 100 MWs or more, are being designed and installed regularly and are financed on a scale of 20-30 years. As part of long-term financing, banks, independent engineers and others must forecast a facilities energy production over that same 20-30 years. Many factors go into the production modeling such as: irradiance modeling, planned maintenance, system degradation, plant availability, and losses due to snow, shading or soiling. PV soiling, energy losses due to dust, dirt, pollen, or other contaminants on the PV module surface, can be as low as 0.5%/year for locations with regular rainfall and clean air or greater than 30%/year in desert locations where it might not rain for months [2, 3]. With such large PV facilities, energy losses due to soiling can equate to millions of dollars of lost revenue. Although soil can be washed or brushed from the PV module surface, the cost of cleaning must be carefully considered in context of the potential revenue gains and the expectation of future rainfall to naturally clean the panels [4]. A key component of this economic optimization are data confirming the soiling losses at a PV facility.

The highest quality soiling data are measured by visiting a facility and measuring current-voltage (I-V) curves on dirty strings of PV modules and then cleaning the strings and repeating the I-V curves to measure the increase of power production. These data can then be used to estimate soiling losses for the entire facility. While these measurements provide very reliable results, they are also very expensive due to labor costs and due to the remote locations of many PV facilities. Due to these high costs many other options have been considered for measuring PV facility soiling losses. For example, the Soiling Rate and Recovery, SRR, algorithm was developed by Deceglie et al [5] to fit soiling losses trends to PV performance data. This method can quickly extract soiling losses for an entire PV facility but application has been limited because the method requires high quality performance and irradiance data. SRR results can have high uncertainty and provide no benefit if the modeled performance index has significant noise. Direct measurements of soiling are typically done at the module or reference cell size scale where one module or reference cell is regularly cleaned while the other module or cell naturally soils [6]. The ratio of the performance of the dirty to clean device is called the soiling ratio, SR, and is a direct measurement of PV soiling. Limitations of this method are: small scales are not always representative of the larger PV facility [7, 8], small mounting misalignment between the two devices can result in an incorrect SR [9], and maintaining the clean cell in the clean state can be challenging for various reasons [10], for example many remote locations have no staff for regular manual cleaning or the wrong device is accidentally cleaned. There are various designs that focus on maintaining the clean cell or module without human labor; for example automatic covers that protect the device from soiling [11] or automatic brushes [12] or water sprays to achieve daily cleaning [13]. Due to limitations and

costs of these devices, in recent years there have been several so called “optical” sensors introduced to measure soiling losses and estimate the SR. Optical sensors share in common that they don’t require regular cleaning and that they don’t rely on the solar irradiance as is the case with side-by-side clean and dirty PV sensors. The MARS sensor by Atonometrics [14], DUST IQ by Kipp and Zonen [15], and DUSST (the focus of this work) [16-19] are all examples of optical soiling sensors. While a single optical soiling sensor does not solve the potential problems of small scale, the intent is to develop sensors that can be deployed in larger quantities due to both high reliability (due to low maintenance) and low cost. Deploying soiling sensors at a larger scale allows for study and understanding of soiling nonuniformity, both across a PV facility or across geographic regions that are expected to have a large quantity of PV installations while also having higher risks for soiling losses. Previous publications on the DUSST sensor have focused on indoor characterization [17-19] with very basic outdoor testing [18]. The focus of the current work is testing DUSST against standard soiling measurements in a range of outdoor locations including: Riyadh in Saudi Arabia, Richmond (Utah, USA), Sacramento (California, USA), Platteville (Colorado, USA), Welby (Colorado, USA), and Globeville (Colorado, USA). The DUSST units tested in California and Saudi Arabia are similar to the device as described in [17-19] while the units tested in Colorado and Utah explore new design variations with the possibility of testing glass coating efficacy for anti-soiling properties. The paper is arranged as follows: 1) Introduction, 2) Methods, design, and prototypes, 3) Indoor Results, 4) Field Results, 5) Discussion, and 6) Conclusions.

2. Methods: Design, Prototypes, and Calibration

2.1 Design

A broad overview of the DUSST sensor is provided in the schematic given in Fig. 1 as well as being described in within the device patent [20].

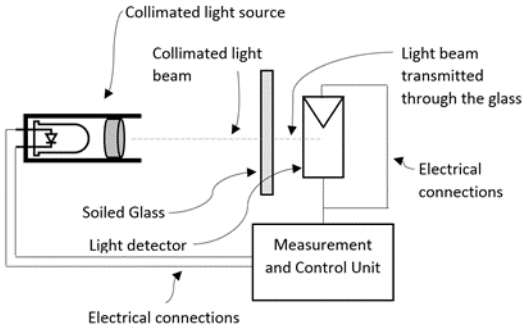

Fig. 1 Schematic of DUSST soiling measurement device.

The basic principle of DUSST is that stabile light emitting diodes (LEDs) replace variable sunlight as the light source while measuring soiling-caused transmission losses. Typical PV soiling measurement equipment requires a side-by-side measurement with a clean PV device for correcting for sunlight variation impacts on the soiled device. The use of a stabile light source removes the requirement to

have both a dirty and clean PV device. The DUSST light source is oriented towards the ground, as shown in Fig. 2, in order to protect the light source surface from soil precipitation due to gravity. The light source is pointed at a light detector which has a top surface that is allowed to naturally soil. The light detector can easily be modified to match the PV technology in the field, for example the semiconductor or the glass surface of the PV panels. In this work DUSST is implemented with an encapsulated silicon solar cell (with a glass top layer) as the light detector. The LED(s) are turned on periodically at night to take measurements of the soiling losses per a mV output from the solar cell biased in the short circuit configuration (also called reference cell Isc). The reference cell baseline Isc is measured in clean conditions with the LED on but no other substantial ambient lighting. The SR is calculated each night outdoors as the reference cell soils naturally. The SR estimate from DUSST is the ratio of the nightly dirty Isc to the clean or baseline Isc (taking into account necessary calibration factors). The baseline clean Isc can be remeasured or calibrated any time the DUSST sensor is determined to be fully cleaned. Any soiling on the light source surface will reduce light reaching the PV cell and in turn will introduce error in SR estimates. For this reason, this work investigates designs with (Fig. 4) and without (Fig. 2) a tubular shroud. The tubular shroud projects from the light source towards the ground with the intent to minimize airflow near the light source surface and therefore reduce the likelihood of airborne particles attaching to the surface. More complete details of the overall DUSST design are described in [17-19] while application to the various semiconductor devices is examined in [21] and [22].

2.2 Prototypes

This work includes field testing of two different prototypes of the DUSST sensor, one with single LED light source (1-LED) and another with a seven LED (7-LED) light source.

2.2.1 1-LED configuration

Atonometrics [13] has been awarded U.S. Department of Energy funding to explore commercialization of the DUSST sensor [20] and is responsible for the build, calibration, and deployment of the 1-LED prototype DUSST sensors presented in this work. This configuration consists of a single 530 nm LED, prepacked with a Fraen 9° concentrating optic from Luxeon Star LEDs. The LED package is powered by the 3021-D-I-700 BuckPuck from Luxeon Star LEDs, a 700mA constant current driver, which is supplied a nominal 12 volts. Atonometrics fabricated a unique support structure and used reference cells and dataloggers that are consistent with their other commercial products. The initial prototype Atonometrics DUSST units intentionally do not have a protective tube around the light source in order to provide baseline lens soiling data for input into the design of a collimating tube to be included in the next stage of design. The Atonometrics test configuration for DUSST is shown in Fig. 2 where the green LED is shown to be illuminating the reference cell. The configuration enables direct comparison to a dirty and clean reference cell pair. Note the image also shows the MARS sensor [14] but this is for Atonometrics internal comparison and is outside the scope of this paper.

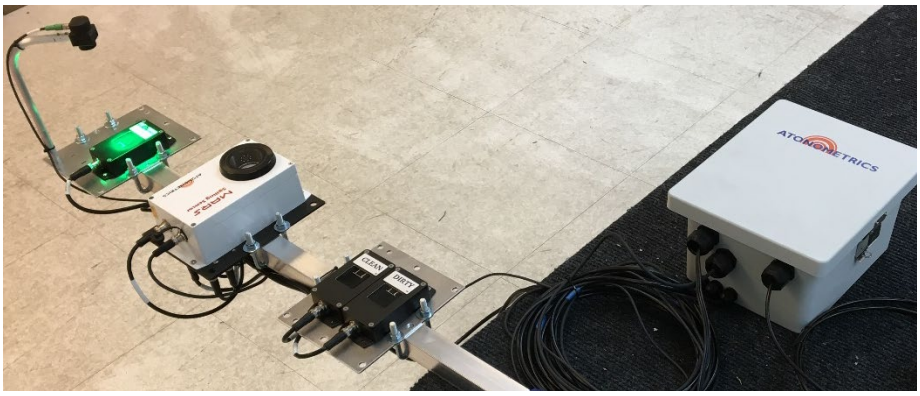

Fig. 2 Atonometrics equipment for testing DUSST side-by-side with a reference cell pair as well at the MARS sensor.

Atonometrics deployed DUSST sensors configured per Fig.2 in both Sacramento, California and at the Sustainable Energy Technologies Center of King Saud University (KSU) in Riyadh, Saudi Arabia. In Saudi Arabia the sensor was calibrated at the beginning of deployment and measurements were scheduled for 10 PM local time. The LED was pulsed on and off for 1 minute with a repeating sequence being 5 s on and 5 s off. The average result over the 1 minute is used to report a single SR per day. This method is intended to prevent significant heating of any of the DUSST components and therefore the components are assumed to be at ambient temperature. No temperature corrections are applied to any of the data from Saudi Arabia. In the California deployment, the LED is cycled 5 s on and 5 s off as in Saudi Arabia but this is done continuously. Nighttime data is determined from daytime data by examining the reference cell output when the LED is off, i.e. if the reference cell has a positive output above a preset noise threshold and the LED if off, the data point is considered part of daytime and this data is not included in the average SR calculations for the given day. For the California unit, Atonometrics also adhered a photodiode directly to the edge of the LED lens for measuring potential variation in light output that can be caused due to temperature variation or noise in the power supply circuit. The results include testing with and without correction using the photodiode output.

2.2.2 7-LED configuration

One of the key results in [19] was that DUSST in the base configuration is best calibrated with piecewise linear model. In the specific DUSST unit tested in [19], the coefficient of calibration was piecewise defined for soiling losses greater than 33% and for losses less than or equal to 33%. This nonlinearity was assumed to be due to the nonlinear behavior of silicon PV cells under the low light conditions associated with using one low power LED. In an effort to increase the output signal and to reduce noise, an alternate prototype of DUSST was built using a 7-LED white light source and an appropriately matching collimating optic. This configuration has the potential to increase light intensity on the reference cell by 5 times or more depending on the operating current and the spacing between the optics and the reference cell.

Figure 3 shows the spectra for the white LEDs in this new build of DUSST as well as pictures off Luxeon's SinkPAD-II 7 Rebel LED 40mm round module. These Luxeon components are not packaged together as in the 1-LED configuration and therefore required assembly. The SinkPAD-II was directly adhered to an aluminum heat sink using thermally conductive epoxy. Soldering was completed per the manufacturer's instructions to operate the 7 LEDs in a series configuration. A polycarbonate collimating lens, made by Polymer Optics, was adhered to the SinkPAD-II with a clear flexible construction adhesive. In the process of attaching the lens, each LED was encapsulated by the adhesive so that only the front

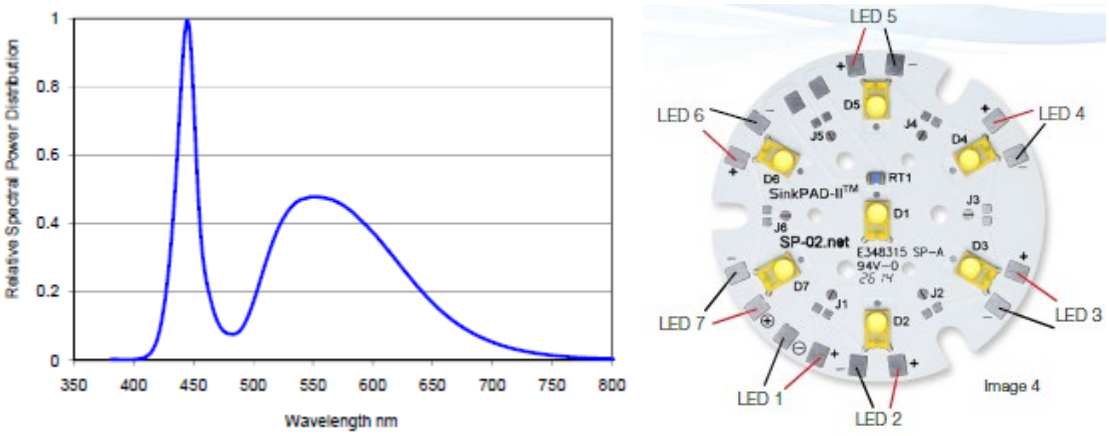

Fig. 3 White LED spectra and 7 LED mounting configuration courtesy of Luxeon Star LEDs.

side of the lens is directly exposed to air. A 51 mm long section of 44 mm diameter (3 mm wall thickness) aluminum tube was also adhered to the heat sink using thermally conductive epoxy. The light source was then coupled to a crystalline-silicon solar cell per aluminum strut. The solar cell was encapsulated at the National Renewable Energy Laboratory (NREL) per 3 mm Solite low iron solar glass, ethylene-vinyl-acetate (EVA) and a typical layered commercial backsheet material (polyvinyl fluoride/ polyethylene terephthalate/EVA), the standard package configuration of full-size solar modules. The distance between the end of the aluminum tube and the cell surface was set to 70 mm. For the Utah unit, the LEDs are powered by Mean Well DDR-120A-12, 12 volt DC to DC converter while the Colorado units use a TRACO TIB 080-112, 120 volt AC to 12 volt DC converter. This difference is due to the need to power the Utah unit with a solar panel, 12 volt battery, and a solar charge controller because no AC power is available at the Utah field site. The Colorado sites have AC power available and hence the TRACO unit converts AC to DC. At both the Colorado and Utah sites, the DC output is trimmed to 14 volts which is fed into a LUXdrive A011-D-V-700. Figure 4 shows the 7-LED configuration as mounted for installation near Richmond, Utah.

DUSST field measurements per the 7-LED configuration are conducted from 10 PM to 4 AM each day. During this period, at the beginning of every 10-minute interval, the LEDs are turned on for 5 s per controls from a Campbell Scientific CR1000 data logger. All data is corrected for ambient temperature

variation, but temperature correction methods vary and are fully described in the section 3.2. As discussed in [18], the DUSST sensor has a clearly distinguishable signal of rapidly declining output when snow accumulates on the sensor. This work is focused on comparing daily SR values, due to dust rather than snow, across different soiling measurement devices and therefore periods of snow accumulation are filtered from the average daily SR reported from DUSST measurements.

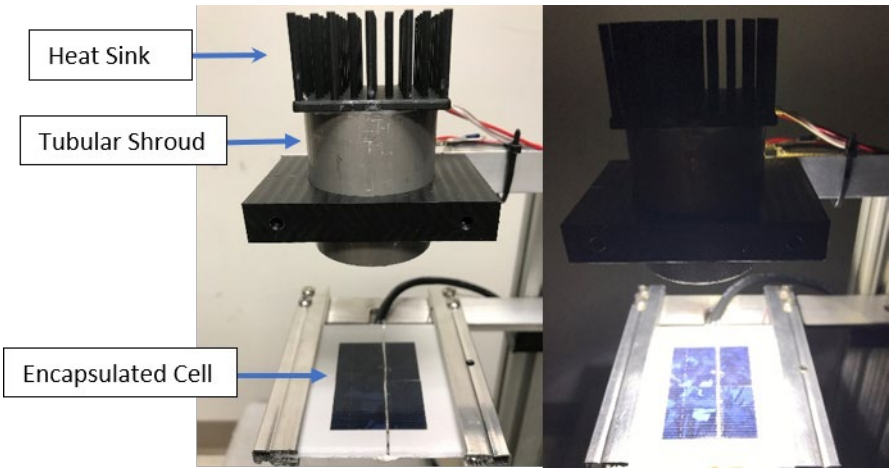

Fig. 4 On the left is the assembled 7-LED configuration where the heat sink, the aluminum tubular lens shroud, and the encapsulated solar cell are easily distinguishable. On the right is the unit with the LEDs on, the light source is sufficiently bright that the solar cell blue color and crystallinity can be distinguished.

2.2.2.1 Nine-Unit, 7-LED configuration for measuring soiling variation

A compact Nine-Unit DUSST sensor (meaning nine individual DUSST sensors packaged together) was designed for examining the potential soiling measurement errors due to using a small-scale device as well as considering different reference cell surfaces. While the specific impact on different reference surfaces is outside the scope of this work, the Nine-Unit design was deployed at 3 locations in Colorado and SR results are presented for these locations. The compact Nine-Unit design is provided in Fig. 5. The tilt of the reference cells was set to 10 degrees (as compared to latitude tilt of 39 degrees) for potentially increasing the soiling rate and gathering nonuniformity data. This is not intended to capture nonuniformity across a large-scale solar field, in this case multiple DUSST sensors would be deployed across the solar field depending on size and geography.

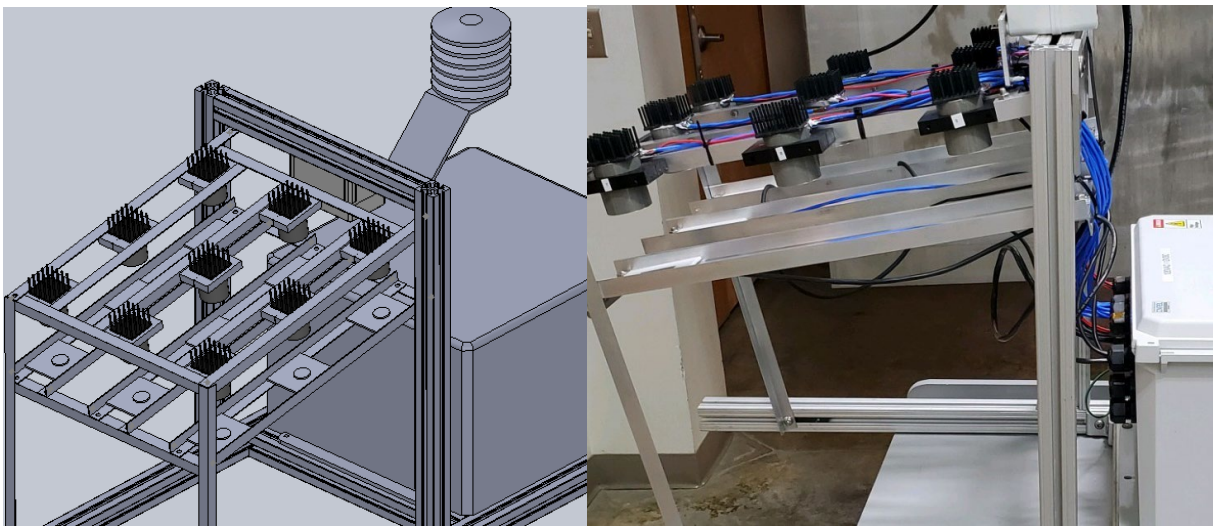

Fig. 5 On the left is a CAD drawing and on the right is the actual build where nine of 7-LED DUSST devices are packaged together to measure soiling variation and to test coating efficacy. Attached to the structure is an outdoor enclosure for holding the datalogger, LED controls, battery, and power supply hardware. At the top of the unit is the housing for holding ambient temperature and pressure measurements.

2.2.3 Prototype deployment summary

Table 1 provides a simple summary of the various protype DUSST units deployed for field testing.

Table 1. Summary information on DUSST units subjected to field testing.

Location	Riyadh, Saudi Arabia	NE Sacramento, California	Richmond, Utah	3 Colorado Cities
Deployment date	June, 2020	July, 2020	October, 2020	September, 2020
Tilt (degrees)	25	38	26.5	10
LED No. and color	1-LED green	1-LED green	7-LED white	7-LED white
Lens shroud	NO	NO	YES	YES
Variation notes	None	Extra: Photodiode attached to lens	Extra: protected reference sensor	9 individual sensors
Measurement process	1 minute of data at 10 PM, pulsed on and off for 5 s intervals	Pulse on and off for 5 s intervals continuously, daytime data excluded using off measurement	10 PM – 4 AM, Every 10 minutes the LEDs are turned on for 5 s	10 PM – 4 AM, Every 10 minutes the LEDs are turned on for 5 s

3. Indoor Results, 7-LED configuration

3.1 Irradiance Calibration

The calibration of the 7 LED DUSST configuration was completed using NREL's Abet solar simulator. The Abet's spectrum and intensity were set using a spectroradiometer, primary reference cells and spectral mismatch correction factors to give the performance under the Global Reference Spectrum (ASTM G173 or IEC 60904-2, 1000 W/m^2 total irradiance). Under these conditions the DUSST encapsulated reference cell was measured to produce 434.75 mV with a measurement uncertainty of 0.8%. Under the same conditions the simulator was also used to measure the reference cell mV output when it was covered with 12 different printed greyscale transparencies. This process was repeated using the DUSST LED and a Campbell Scientific CR1000 data logger. The maximum output of the DUSST, no grey transparency, equates to 423 W/m^2 in relation to the solar simulator. Both the simulator measurements and the DUSST measurements were normalized to 1 and are plotted against each other along with the line of best fit, R^2=0.999, in Fig. 6. As compared to the results in [19], the 7-LED DUSST unit does have the targetted 5 fold increase in light intensity and therefore a higher signal to noise ratio. This is demonstrated through Fig. 6., where a single linear calibration coefficient can accurately measure SRs as low as 0.25 (a 75% reduction in PV output). While a darker transparency would be needed to demostrate further linearity, there is no practical need to measure PV soilng losses greater than 75% as maintained PV facilities are typically cleaned before soiling reaches such an extreme level

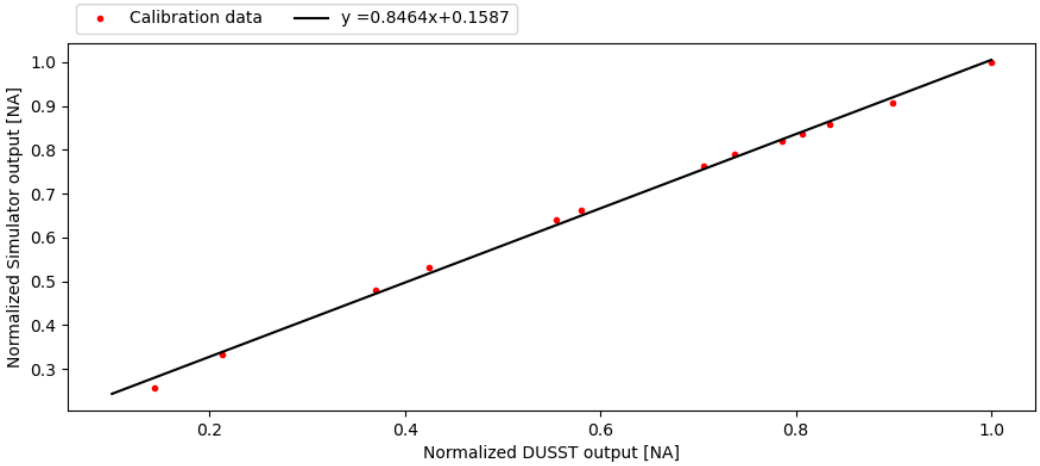

Fig. 6 Calibration of the 7-LED DUSST unit comparing normalized DUSST output against normalized solar simulator output, where the same reference cell Isc is measured clean and under 12 different greyscale transparency masks.

3.2 Temperature calibration

Individual temperature dependencies of the components in previous builds of DUSST were explored in [19] in the range of 25 °C to 45 °C and considering the LED would be turned on for 10 minutes or more. While this was relevant for laboratory testing, in the field testing in this work, the longest period of turn

on is 5 seconds and nighttime winter temperatures in both Utah and Colorodo can be well below 0 °C. For this reason we examine overall temperature dependencies in the range of -20 °C to 40 °C. There are a number of components that have potential temperature interactions and the total response is complex and not the subject of this research. Hereafter we list the various possible temperature dependencies for the readers consideration but we only provide test results on the total response of the device system within a thermal chamber. Possible temperature dependencies as well as manufacture data are given in Table 2.

Table 2. 7-LED DUSST components with potential temperature dependencies

Item with potential temperature dependency	Manufacturer information
LED voltage	-0.1 %/°C
Reference cell Isc	+0.06 %/°C
Resistor across reference cell	-0.0005 %/°C (for -15 to 25C, positive above 25 °C)
12 or 24 V (AC to DC converter)	Not listed
Optical package focal length	Not listed
SinkPAD-II 7 Rebel LED 40mm package	Not listed
TRACO TIB 080-112 AC to DC converter	+/-0.02%/°C, load variation 0.5% max
Mean Well DDR-120A-12 DC to DC converter	+/-0.03%/°C, load regulation is +/-1%
LUXdrive A011-D-V-700 constant current driver	Not listed

Both the Utah unit and Colorado units were operationally tested in thermal chambers before field deployment. Due to the extreme cold conditions expected for these units, the data logger enclosures were insulated and heaters were included in the enclosures to keep inside air above freezing to prevent condensation on the electrical equipment. Enclosure heaters were operational during thermal testing and the condensed results of one of the Colorado units is shown in Fig. 7. The red-dashed data given in Fig. 7 is chamber ambient temperature versus the normalized output from the Colorado DUSST reference cells. The chamber was held at each ambient temperature condition for multiple hours until the DUSST heat sink temperature and cell temperature were at steady-state with ambient temperature. Components inside the enclosure did not go below freezing but ranged from 10 °C to 40 °C depending on ambient conditions. The nine individual DUSST sensors within the Colorado unit all showed a similar quadratic trend with ambient temperature therefore the mean of the nine sensors was considered for determining the equation for making temperature corrections, “DUSST all heated” in Fig. 7. As can be seen in Fig. 7., the quadratic equation given provides a near perfect fit for “DUSST all heated” and hence the equation shown is used for temperature correcting field data in Colorado.

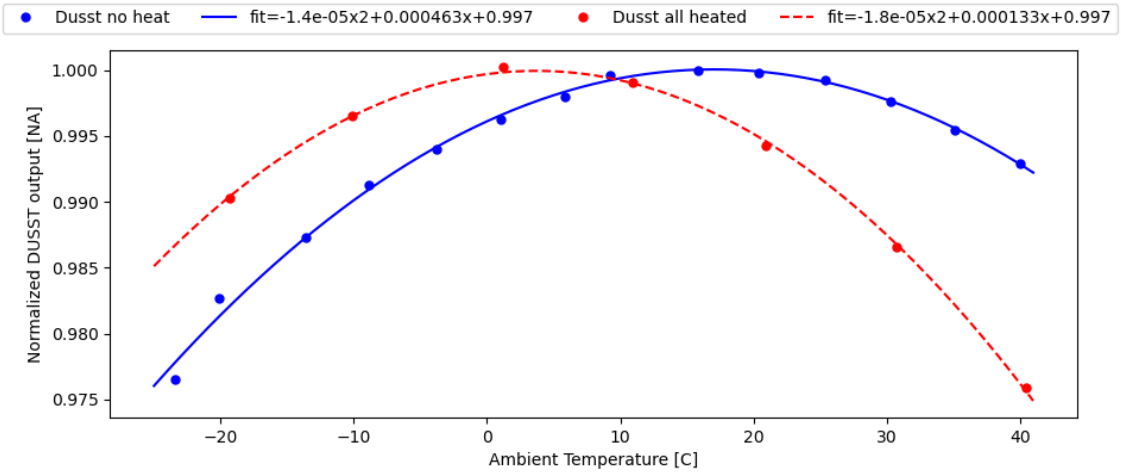

Fig. 7 Chamber ambient temperature verses normalized DUSST output: In red is the normalized mean of the nine reference cells from one of the mulit-unit DUSST systems deployed in Colorado where the electronics enclosure is heated during thermal testing. In blue is the normalized result from another single DUSST sensor that includes a photodiode on the lens and no heating was provided to the electronics enclosure during thermal testing.

Results for thermal testing of the Utah unit showed a similar quadratic behavior to what is shown in Fig. 7 but the data were significantly noisier. Careful examination of the data suggested that turn on events for the enclosure heater were correlated with temporary declines of the LED output. While the data were not sufficient to prove the exact cause, it is thought that solar charge controller (controls load as well) was impacted at the turn on of the heater load and hence impacted the DC supply to the LED circuit. Due to this noise being unacceptably high, the Utah unit was modified to include two DUSST sensors where the second is protected from soiling but exposed to ambient temperature as shown in Fig. 8. Both DUSST sensors are powered at the same time and therefore the second protected sensor can be used to remove noise from the soiled signal.

An additional chamber test was conducted on another 7-LED DUSST unit with two modifications from the field deployed units: 1) The enclosure was not heated and 2) a photodiode was adhered to outer front edge of the polycarbonate optic. In this test, power was supplied to the battery from a direct plugin in AC to DC converter that was exposed to ambient chamber conditions. These results, for comparison with the Colorado unit thermal testing are provided by the blue-solid line in Fig. 7. In both cases, the normalized DUSST output has a strong quadratic relationship with ambient temperature but the peak output shifts from 3 °C to 17 °C for the sensor with an unheated electronics enclosure. For the DUSST sensor with an unheated enclosure test, Fig. 9 shows that photodiode output linearly increases with temperature and Fig. 10 shows that the DUSST output is quadratically related to the photodiode output. Figures 9 and Fig. 10 together suggest that the primary driver of DUSST output changes are due the optical focal length changing with temperature. The photodiode output demonstrates that light intensity at the lens surface is continually increasing with temperature even while the light reaching the

solar cell is decreasing. This is possible if the focal length is changing and causing more light to spill outside the boundaries of the solar cell. This is possible due to temperature dependent mechanical deformation and the temperature dependent optical refraction index. The output angle of refractive optics is given by the shape and refractive index of the material. When temperature changes, the refractive index at each wavelength is modified, and as a consequence, the output angle is also modified. Similar behavior has been modeled and experimentally validated for concentrating PV modules with various lens types and materials [23-29].

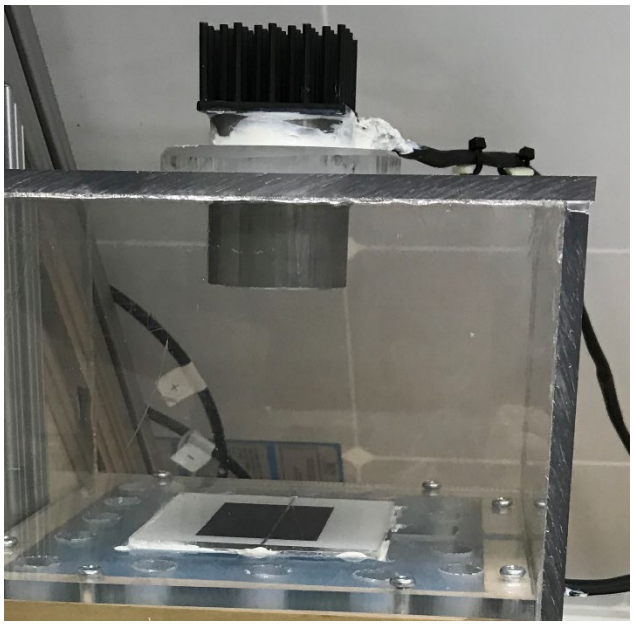

Fig. 8 The Utah field test has two DUSST sensors, one as shown in Fig. 4 and the second as shown here is protected from soiling by a plastic box. Ambient air is allowed to pass through a filter at the bottom of the box to avoid pressure changes or condensation within the protective box.

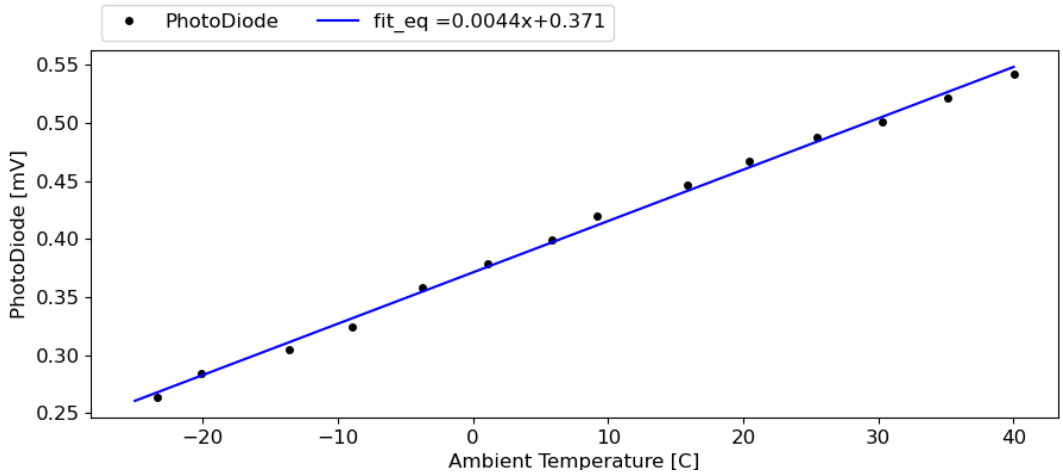

Fig. 9 Results from a photodiode adhered to the edge of the polycarbonate optic show that the photodiode output (light intensity at the lens surface) increases linearly with chamber ambient temperature, which in this test is also the temperature of the DUSST sensor, solar cell, and supporting electronics.

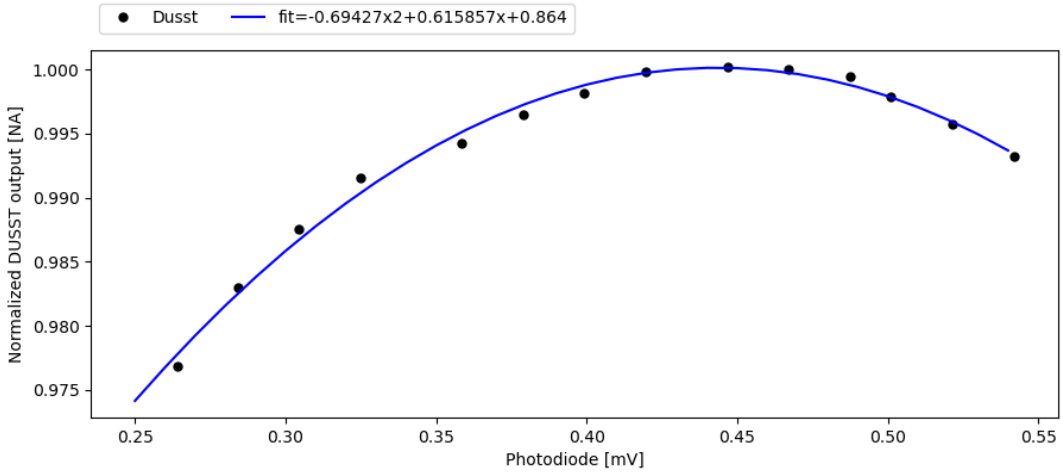

Fig. 10 DUSST output is quadratically related to photodiode output (light intensity at the polycarbonate lens surface) suggesting that the explanation behind the quadratic temperature response of the 7 LED DUSST configuration is due to the temperature dependence of the optical focal length.

4. Field Results

4.1 Utah

The Utah field site is near the rural town, Richmond, which is generally surrounded by agricultural fields. The site includes soiling measurements on multiple full-size PV panels pairs (1970 mm by 990 mm) which include commercial antireflective surface coatings. The clean full-sized panels are manually cleaned every weekday. All soiling measurements at the site, including DUSST, are set to 26.5 degrees

tilt. On of October 16, 2020, all systems were cleaned to provide an equal starting point. Figure 11 shows detailed data from the DUSST sensor, including ambient temperature, the reference and soiled DUSST measurements, and the corrected output. The reference sensor shown in yellow is observed to move up and down with ambient temperature and, as expected, not to soil. The uncorrected DUSST in blue shows a clear downward soiling trend but shows noise and movement with ambient temperature. The black corrected DUSST data, blue divided by yellow, show significant noise reduction and removal of temperature dependence.

Figure 12 shows snow events and the daily corrected DUSST SR in comparison to daily SR from 2 sets of full panel pairs. SR data for the first full panel pair, yellow, is reported directly per the manufactures proprietary filtering algorithm. In red is the daily SR from the second full pair where the SR is the median ratio of the data from 11 AM to 1 PM where the GHI is greater than 500 W/m^2 (to eliminate noise due to potential small misalignment of the modules as well as noise from low irradiance data). On October 24th no data is shown for the full panel SRs because there were no measurements with the GHI above 500 W/m^2. The DUSST measurement is taken at night and does not rely on irradiance and hence is still shown. The slopes and their standard error for linear fits for each data set in Fig. 12 are -0.099 %/day ±0.006 (SR1), -0.088 %/day ±0.001 (SR2), -0.110 %/day ±0.004 (DUSST). Light snowfall was recorded on October 25th and 26th coinciding with little change in the soiling ratio on these days for all three measurements. On November 8th a snowfall event is shown that aligns with different changes in SR for each of the sensors. Further investigation of this event showed that the precipitation was a mix of rain and snowfall which could explain why there is not a more systematic recovery in SR for all 3 measurement systems. Experience of the authors has demonstrated that snow does not typically provide consistent slide-off cleaning of glass surfaces as small as the DUSST reference cell (a 76 by 76 mm glass surface). The melting of the snow and the drying of a surface is complex and depends on size, tilt, and the meteorologic conditions at the time.

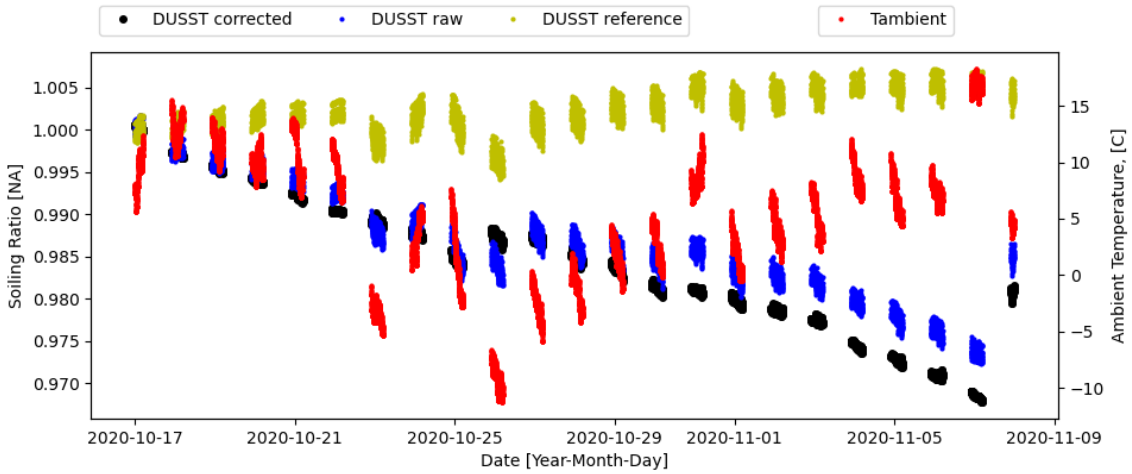

Fig. 11 Measurements are taken every 10 minutes at night for 5 seconds at 1 second interval. Each grouping of data points is presenting the data for the entire night. In red is the ambient temperature shown to range from -12 to 17 °C. In blue are data from the DUSST that is naturally soiling while in yellow is the DUSST sensor within the plastic box. The black data are the result of dividing the blue, "DUSST raw", by yellow, DUSST reference.

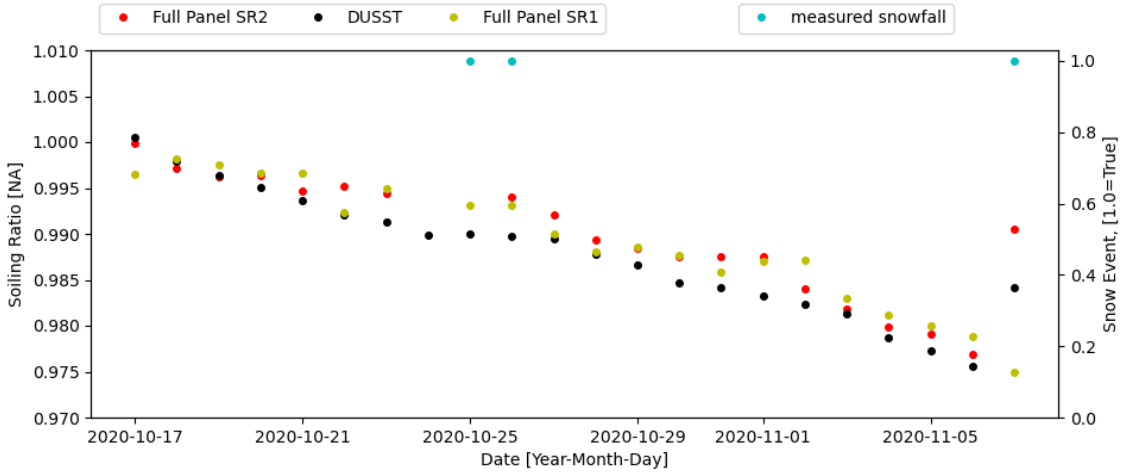

Fig. 12 Single daily SRs from DUSST, black points, compared to SRs from two different full size module pairs.

4.2 California

The California field site is just to the northwest of Sacramento and while it could experience urban pollutants from Sacramento, it is generally surrounded by agricultural fields. The DUSST and reference cell equipment was provided by Atonometrics and are coaligned per Fig. 2. The clean reference cell is irregularly manually cleaned due to lack of regular personnel on the site. For this reason, reference cell SR data is only retained for days where cleaning is demonstrated by an upward shift in the clean cell data. Figure 13 provides a 3-month soiling loss trend and the data comparison between the reference cell SR and DUSST SR both before and after correction with output from the photodiode on the DUSST lens. The least-squares linear fit soiling rate for the 3-month period is -0.19%/day for the corrected DUSST measurements and -0.20%/day for the reference cell SR data.

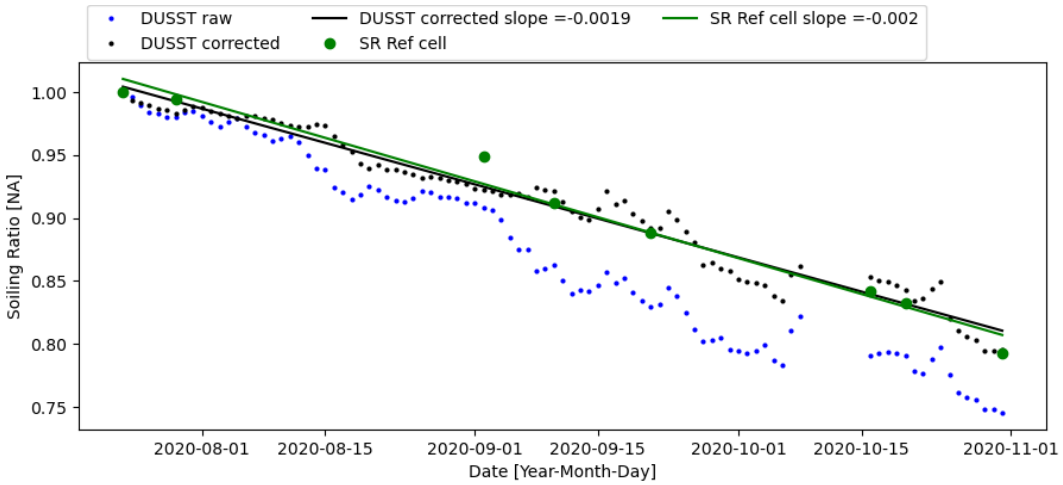

Fig. 13 A 3-month period with growing soiling losses near Sacramento, California. The green dots are reference cell SR values for days when cleaning is conducted for the clean cell only. Blue dots are uncorrected DUSST data and black dots are DUSST data corrected using the photodiode adhered to the lens. Slopes and the least squares linear fit are provided for both the reference cell and corrected DUSST data.

4.3 Riyadh, Saudi Arabia

Riyadh, Saudi Arabia typically has airborne particulate matter concentrations that are 5-10 times higher than the deployment sites in the United States and therefore this site provides the opportunity for extreme soiling.

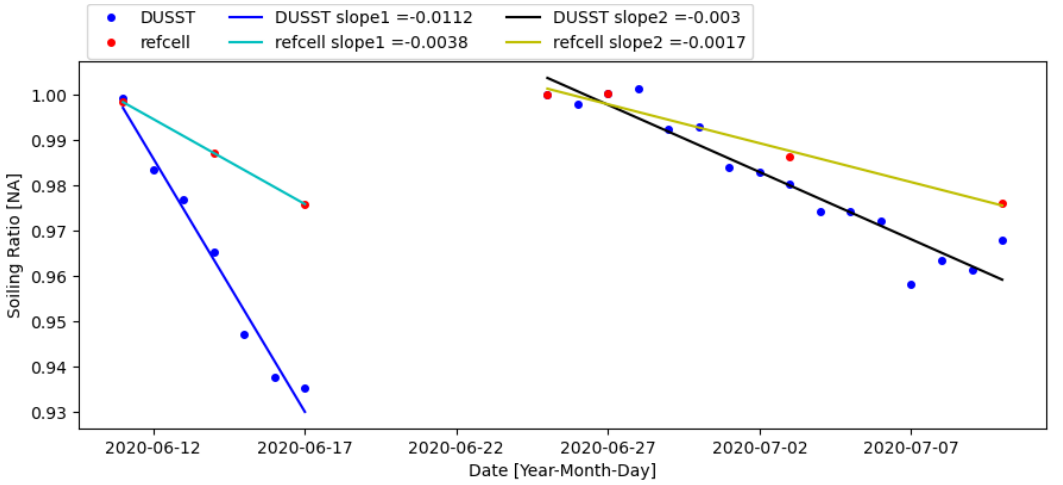

Fig. 14 Reference cell SR data are shown per red dots for days with confirmed cleanings while DUSST data are shown with blue dots. Both the reference cells, the DUSST solar cell, and the DUSST lens where all cleaned on June 25th to reset the soiling measurements. Data in between the June 17th and the 25th are not shown because there were no reference cell data points in this period with confirmed cleanings.

The DUSST sensor configuration as shown in Fig. 2 was deployed on June 11th as shown in Fig. 14. The clean cell was manually cleaned 2-3 times per week and the data in between cleanings was typically noisy. For this reason, only data immediately following confirmed cleanings were retained. The soiling trend beginning on June 11th is significantly higher than the trend that starts on June 25th, as measured by both DUSST and the reference cell pair. Both soiling trends show DUSST output reducing at a higher rate than the reference cell rates, -0.38%/day and -0.17%/day respectively. In both cases the lens was confirmed to visually show soiling and therefore this is a partial explanation for the higher soiling rates per fits to the DUSST data. Unfortunately, the level of lens soiling was not measured coinciding with the June 25th cleaning. In the second soiling trend the last reference cell measurement shown is on July 10th. On this date, the difference between the DUSST and the reference cell fits is approximately 2%. Four days later, on July 14th the DUSST lens was cleaned and the resulting DUSST performance increase was 3.7% (lens soiling measurements are described in section 4.5). This suggests, for the second soiling trend, lens soiling could be a partial explanation of the difference between DUSST and reference cell SR measurements. Other possible sources of error come from lack of a specific SR and temperature calibrations for the device build in Saudi Arabia.

4.4 Colorado

The Nine-Unit, 7-LED configuration for measuring soiling variation was deployed in Welby, Globeville, and Platteville, Colorado. The Welby site is in the northern metropolitan Denver area is expected to be impacted a mix of urban and industrial pollution but the immediate surroundings of the site are the Platte river, a horse farm, and open fields. The Globeville site is located along the Denver Interstate 25 corridor and is one of the heaviest measured urban pollution areas in Colorado. Specially this station is within 10 m of heavy traffic flow and experiences turbulent air flow due to traffic and heavy pollution from automotive exhaust. Previous deployments by NREL at the Globeville site have also demonstrated that equipment at the site is exposed to dirty mist generated by traffic flow on wet pavement as well snowplow tailings when road crews are removing snow from Interstate 25. While these aspects of Globeville are not representative of typical PV sites, it does provide an extreme test for equipment reliability and potential lens soiling. The Platteville site is more representative of the rural semi-arid environment of the eastern plains of Colorado. Figure 15 provides data for six DUSST sensors (the three measurements using anti-soiling coatings have been excluded) at Welby for a month-long soiling trend starting on September 9, 2020.

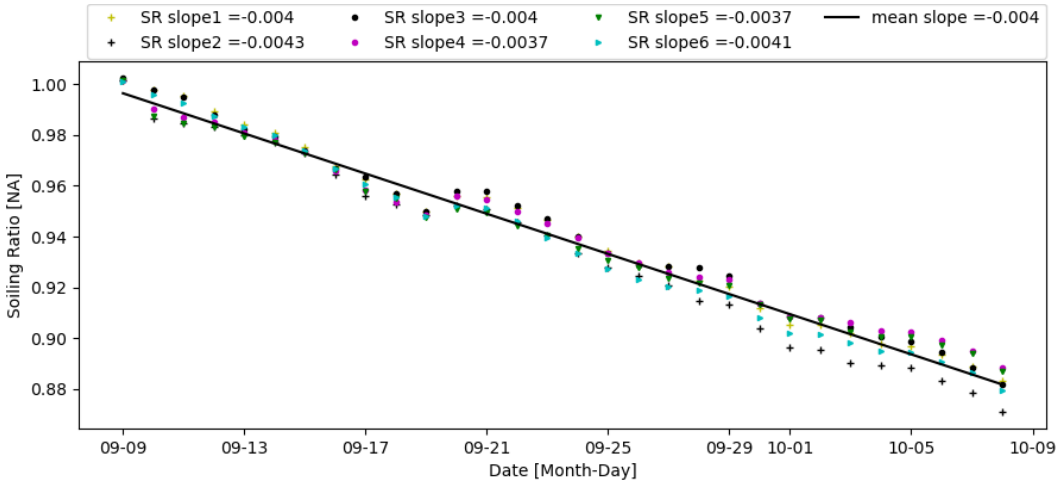

Fig. 15 Daily SR are shown for six of the nine 7-LED DUSST sensors in Welby, Colorado as well as the mean soiling rate.

The Welby station shows a mean loss from the six sensors of 11.8% after one month but some of this loss is attributed to lens soiling to be detailed in section 4.5. The variation in the soiling rate is shown in the legend ranging from 0.37%/day to as high as 0.43% per day. Variations are potentially due to measurement error or from the expected nonuniformity of soiling for an area of 0.5 m by 0.5 meter and the soiling area per solar cell of about 4 cm by 4 cm. Graphical data are not shown for the other two sites in Colorado but all 3 sites showed clear linear soiling trends. The mean soiling rates were 0.46%/day for Globeville, 0.40%/day for Welby, and 0.31%/day for Platteville where Globeville and Welby were measured from September 9th through October 9th and Platteville was measured from September 24th through October 13th (the longest soiling period at Platteville with no snow or rain). The range of SRs for each site after 3 weeks of continuous soiling is provided in Table 3.

Table 3. SR ranges for each Colorado site after 3 weeks of continuous soiling.

Site	Minimum SR	Maximum SR	SR range
Globeville	0.862	0.880	1.8%
Welby	0.913	0.924	1.1%
Platteville	0.922	0.957	3.5%

4.5 Lens soiling measurements

DUSST was deployed in Saudi Arabia and California with no lens shroud while the 3 Colorado sites and the Utah site all have 51 mm long shrouds. Neither design was optimized to prevent lens soiling, but rather are simple configurations meant to gather data to aid understanding for commercial DUSST designs. Results from California and Utah in Fig. 12 and Fig. 13 show that DUSST SRs closely match other SRs at those sites and therefore suggest that lens soiling has not been substantial. For all three

Colorado sites lens soiling measurements were conducted as follows: All measurements were taken during the daytime per the system datalogger. First the solar cells were cleaned and then the nine-unit DUSST system was covered with heavy black cloth to prevent daytime irradiance from reaching the DUSST sensors. At this point multiple measurements were taken with both the LEDs turned on and off. The cloth was then removed and the lenses were each cleaned. The black cover was then put in place again and multiple measurements were repeated. Lens losses were calculated as the gain between the lens soiled measurement and the lens clean measurement. The whole procedure was conducted over 30 minutes while ambient temperature was stable. In Saudi Arabia, the DUSST lens was cleaned in the daytime on particular days while the solar cell was left to naturally soil. The increase in DUSST performance per the nighttime measurement following lens cleaning was used as an estimate of lens soiling losses. This estimate is expected to be in error by the daily soiling rate of the solar cell when the cleaning took place. On two dates during testing in Saudi Arabia both the lens and the solar cell were cleaned. Per the first date the DUSST output returned to baseline output while on the second date the output increased to several percent above the baseline output. This output increase could not be directly explained by a temperature change and therefore the cleaning of the lens and cell was suspected to mechanically change the spacing or alignment between the lens and the solar cell. No data was used after this date but this unexpected performance shift is a result worth considering in the commercial design phase. Table 4 presents measurements of the increases in DUSST outputs after various lens cleanings, the total losses per DUSST just before cleaning, as well as the time period the lens was exposed. The data is provided in Table 4 for ease of readability and is not intended for intercomparison as each site has unique soiling characteristics and the DUSST equipment in Saudi Arabia does not match the Colorado sites. No data is provided in Table 4 for California or Utah because lens cleanings have not been conducted at these sites. All 3 Colorado sites experienced significant snow events during the time period reported in Table. 4. First, Welby and Globeville had a partial snow cleaning (2-3%) of all reference cells on October 10th. Then on October 26th all 3 sites experienced snow, where this event resulted in improvements of ~2% for Platteville and Welby but Globeville decreased in performance by as much as 20%. A site visit confirmed that all nine DUSST sensors at Globeville was covered by grit and grime from snowplow tailings.

Table 4. Data for lens soiling losses

Site and cleaning date	Weeks of exposure	Lens soiling loss	Total loss measured when lens was cleaned
Platteville, November 17th	7 weeks	1.2-3.2%, 9 devices	7-10%, 9 devices
Riyadh, July 14th	2.5 weeks	3.7%	5.5%
Welby, November 10th	8 weeks	2.1-4.3%, 9 devices	15-18%, 9 devices
Globeville, November 10th	8 weeks	5.8-8.6%, 9 devices	33-49%, 9 devices

4.6 Minimizing DUSST performance variation or uncertainty

In this section we outline the uncertainty associated with the DUSST light source and demonstrate that a significant reduction in uncertainty can be achieved using corrective measures. DUSST SR values are based on the ratio of soiled measurements to the baseline device output. In order to achieve low uncertainty in each SR calculation, variation in light output due to temperature or other factors must be minimized or corrected within the SR calculation. Figure 7 in section 3.2 demonstrated that over the range of -20 to 40 °C ambient temperature, the 7-LED DUSST output could vary ~3% but this variation could be modeled and corrected for using a quadratic fit. An identical chamber study on the solar/battery powered 7-LED DUSST suggested that the activation of the enclosure heater could cause unexpected variation in the DUSST light output and therefore this unit was deployed to Utah with a protected reference sensor (pictured in Fig. 8). While the Utah results demonstrated that using a protected reference sensor reduces error and uncertainty due to temperature variation, heater activation, or other unknown factors it is useful to quantify the error in the data before and after the division by the reference DUSST measurement. To estimate the reduction in error, the true daily SR is temporarily assumed to be the mean of the daily corrected SR. Using this assumption, the standard deviation of the error is 0.04% for the corrected data and 0.24% for the uncorrected data. At two standard deviations this equates to the uncorrected error being ±0.5%, unacceptable when considering soiling losses at many PV facilities are in the range of 0-5%. This demonstrates that applying corrections is essential but when achieved the error at 2 standard deviations can be reduced to less than ±0.1%.

5. Discussion:

5.1 Calibration and field test lessons

Calibration and field test results of protype units of the DUSST sensor provide many data that are valuable in the process of designing a commercial version of DUSST that is durable and provides low uncertainty SR measurements. The early laboratory testing of DUSST in [19] suggested that using a low power LED could accurately measure SR but would require two different calibration coefficients, one for DUSST output below 33% of the baseline and one for above 33%. The new higher light output 7-LED design tested in this work shown in Fig. 6 demonstrates that DUSST can be designed with a single calibration coefficient and that the uncorrected output only slightly overestimates SR values. Thermal chamber results show that the 7-LED DUSST output varies quadratically with ambient temperature (Fig. 7). DUSST chamber results enabled temperature correction of field data but photodiode test data combined with DUSST output data also suggested that this temperature dependence is likely due to changing optical properties, including changes in the refraction index or temperature dependent mechanical deformation. The CPV industry put significant resources into understanding similar optical performance dependencies [23-29] that can guide future versions of DUSST. For example, both versions of DUSST that have been tested in this work allow light to spill outside the active solar cell region. As focal length changes, this implies that the amount of spilled light is changing and hence changing the baseline output. A simple design change can be to use reflective optics or provide a collimating tube to

minimize spilled light. Alternate options can also be tested that use other materials that are less sensitive to temperature changes.

Chamber testing at NREL as well as field testing of DUSST in Saudi Arabia revealed that when electrical circuitry (activation of enclosure heaters) or mechanical design (potential changing alignment between lens and cell) are not carefully considered, undesired shifts or noise can occur in DUSST measurements. At the same time, a reference DUSST sensor was demonstrated to reduce undesired measurement noise and therefore the field unit deployed in Utah demonstrated daily soiling measurements almost identical to full size module measurements where soiling rates over three weeks were -0.10 %/day (full module SR1), -0.09 %/day (full module SR2), and -0.11 %/day (DUSST), (Fig. 11 and Fig. 12). Similarly, a photodiode was used to measure light output at the DUSST lens surface and to correct SR measurements, resulting in the 3-month soiling rate being -0.19 %/day with DUSST and -0.20%/day with a reference cell pair (Fig. 13).

While temperature corrections, photodiodes, and reference measurements can all improve measurement accuracy, lens soiling was measured in Saudi Arabia and Colorado that directly increase uncertainty. The Globeville, Colorado site was the worst case for lens soiling with 5.8-8.6% losses per 9 different lenses after two months of outdoor exposure; where on average lens losses were 24% of the total soiling losses at the time of cleaning. These levels should be considered extreme due to the unusual aspects of the Globeville site that are not experienced at typical utility-scale PV sites: 1) turbulent air from highspeed traffic within 10 m of the DUSST equipment, 2) Sticky hydrocarbon pollution from gasoline and diesel exhaust, 3) dirty mist from tires crossing wet pavement, and 4) snowplow tailings that eject a similar dirty mist and grit directly onto the DUSST equipment. Alternatively, in Saudi Arabia where no protective lens shroud was applied, lens losses were 67% of the total losses compared to the 24% at Globeville. While Saudi Arabia and Globeville cannot be directly compared due to different soiling characteristics and different equipment, the results are consistent with the physical expectation that a lens shroud should reduce lens soiling. Alternatively, even with the current shroud, lens soiling is too high and DUSST must undergo further design optimization to provide reliable soiling loss measurements. Both the Globeville and Saudi Arabia sites provide excellent opportunities to validate the effectiveness of high aspect ratio collimating tubes, lens shutters, or other designs intended to protect the DUSST light source.

5.2 Design directions

Current work at Atonometrics is focusing on DUSST designs that minimize sensitivity to temperature and other factors while incorporating positive results from field testing. The next build to be tested will include a high aspect ratio collimating tube with a narrow opening. This will serve to protect the light source from soiling while ensuring that the light beam is almost completely captured by the detector, potentially also reducing sensitivity to beam alignment. The light source will use a reflector with a single high-power LED rather than a lens with multiple LEDs. A white LED will be employed as this more closely matches the solar spectrum but single wavelength LEDs can easily be tested consistent with research in

this area [21, 22]. A flash circuit or pulsed light will be used to minimize power consumption. This makes the sensor more practical for battery powered meteorological stations. This design also significantly reduces heat generation and therefore no heat sink is required. The commercial version will have an integrated microcontroller control circuit and firmware, allowing ease of use with any datalogger.

6. Conclusion:

Two versions of the DUSST optical soiling sensor where subjected to field testing at differing sites which included Saudi Arabia, California, Utah, and Colorado. Calibration and temperature performance of the baseline sensor with a single 530 nm LED was discussed in previous work while a new DUSST unit with 7 white LEDS and a polycarbonate collimating optic is subjected to calibration and temperature testing in this work. The new design increases light intensity fivefold and demonstrates a single linear calibration coefficient is effective to measure soiling losses as high as 75%. Results show that the performance of the 7-LED optical design varies quadratically with ambient temperature but that this variation can easily be corrected, either directly with a quadratic equation or with a reference device that is operated in parallel with the soiled DUSST sensor.

Field data from Utah and California demonstrated that daily soiling loss measurements and soiling rate calculations closely matched both reference cell and full-size solar panel measurements of soiling losses and soiling rates. Corrective methods employed on the Utah DUSST sensor suggest that it is possible to achieve measurement errors as low as ±0.1% at two standard deviations. Field data from both Colorado and Saudi Arabia demonstrated that LED lens soiling can occur and that design improvements must focus on lens protection. The lesson learned from all the field deployment locations are leading to design improvement which include a high aspect ratio collimating tube to better control illumination on the DUSST detector as well as protect the LED optics from soiling. The next design iteration will also include an integrated micro controller and optimization of the power supply circuitry to allow ease of us with battery powered meteorological stations and any data logger.

7. Acknowledgements:

The authors would like to thank Lin Simpson for his efforts to oversee funding that made this work possible, Byron McDanold, Josh Parker, Josh Morse, and Greg Perrin that provided discussion and technical support to build and deploy various equipment, and Zeyad Abdulwahed who supported testing at KSU in Saudi Arabia.

This work was authored in part by Alliance for Sustainable Energy, LLC, the manager and operator of the National Renewable Energy Laboratory for the U.S. Department of Energy (DOE) under Contract No. DE-AC36-08GO28308. Funding was provided by the U.S. Department of Energy's Office of Energy Efficiency and Renewable Energy (EERE) under Solar Energy Technologies Office (SETO) Agreement Number 35893. This material is partially based upon work supported by the U.S. DOE, SETO under Award Number DE SC0020012." The views expressed in the article do not necessarily represent the views of the DOE or the

Leonardo Micheli was funded through the European Union's Horizon 2020 research and innovation programme under the NoSoilPV project (Marie Skłodowska-Curie grant agreement no. 793120)

Alvaro F. Solas is supported by the Spanish ministry of Science, Innovation and Universities under the program "Ayudas para la formación de profesorado universitario (FPU), 2018 (Ref. FPU18/01460)". Eduardo F. Fernandez thanks the Spanish Ministry of Science, Innovation and Universities (RYC-2017-21910).

8. References:

[1] Renewable capacity highlights 31 March 2020, International Renewable Energy Agency, [Online]. Available: https://irena.org/-/media/Files/IRENA/Agency/Publication/2020/Mar/IRENA_RE_Capacity_Highlights_2020. [Accessed: 14-Dec-2020].

[2] S. Costa, A. Diniz, L. Kazmerski, Solar energy dust and soiling R&D progress: Literature review update for 2016. Renew. Sustain. Energy Rev. https://doi.org/10.1016/j.rser.2017.09.015

[3] S. Costa, A. Diniz, L. Kazmerski, Dust and soiling issues and impacts relating to solar energy systems: Literature review update for 2012–2015. Renew. Sustain. Energy Rev. 63, 33–61. https://doi.org/10.1016/j.rser.2016.04.059

[4] Ilse, K., Micheli, L., Figgis, B.W., Lange, K., Daßler, D., Hanifi, H., Wolfertstetter, F., Naumann, V., Hagendorf, C., Gottschalg, R., Bagdahn, J., 2019. Techno-Economic Assessment of Soiling Losses and Mitigation Strategies for Solar Power Generation. Joule 2303–2321. https://doi.org/10.1016/j.joule.2019.08.019

[5] M. Deceglie, L. Micheli, M. Muller, Quantifying Soiling Loss Directly from PV Yield. IEEE J. Photovoltaics 8, 547–551. 2018, https://doi.org/10.1109/JPHOTOV.2017.2784682

[6] M. Gostein, T. Duster, C. Thuman, Accurately measuring PV soiling losses with soiling station employing module power measurements. 2015 IEEE 42nd Photovolt. Spec. Conf. PVSC 2015. https://doi.org/10.1109/PVSC.2015.7355993

[7] M. Gostein, J. Caron, B. Littmann, Measuring soiling losses at utility-scale PV power plants. 2014 IEEE 40th Photovolt. Spec. Conf. PVSC 2014 885–890. https://doi.org/10.1109/PVSC.2014.6925056

[8] M. Valerino, M. Bergin, C. Ghoroi, A. Ratnaparkhi, G. Smestad, Low-cost solar PV soiling sensor validation and size resolved soiling impacts: A comprehensive field study in Western India. Sol. Energy 204, 307–315. https://doi.ord/10.1016/j.soler.2020.03118.

[9] L. Micheli, D. Ruth, M. Deceglie, M. Muller, Time series analysis of photovoltaic soiling station data: version 1.0, August 2017. Golden, CO: 2017.

[10] Muller, M., Micheli, L., Martinez-Morales, A.A., 2017. A Method to Extract Soiling Loss Data from Soiling Stations with Imperfect Cleaning Schedules. 2017 IEEE 44th Photovolt. Spec. Conf. PVSC 2017 1–6. https://doi.org/10.1109/PVSC.2017.8366214

[11] T. Curtis, S. Tatapudi and G. TamizhMani, "Design and Operation of a Waterless PV Soiling Monitoring Station," 2018 IEEE 7th World Conference on Photovoltaic Energy Conversion (WCPEC) (A Joint Conference of 45th IEEE PVSC, 28th PVSEC & 34th EU PVSEC), Waikoloa Village, HI, 2018, pp. 3407-3412, doi: 10.1109/PVSC.2018.8547820

[12] S.Toth, M. Hannigan, M.Vance, andM.Deceglie, “Enhanced photovoltaic soiling in an Urban environment,” in Proc. IEEE Photovolt. Spec. Conf., Chicago, IL, USA, 2019, pp. 2904–2907.

[13] Atonometrics, “Soiling Measurement System for PV Power Plants.” [Online]. Available: http://www.atonometrics.com/products/soiling-measurement-system-for-pv-modules//. [Accessed: 14-Dec-2020].

[14] M. Gostein, S. Faullin, K. Miller, J. Schneider, B. Stueve, Mars Soiling Sensor ™, in: 7th World Conf. Photovolt. Energy Convers., IEEE, Waikoloa, HI, 2018, https://doi.org/10.1109/PVSC.2018.8547767

[15] M. Korevaar, J. Mes, P. Nepal, G. Snijders, X. van Mechelen, Novel Soiling Detection System for Solar Panels, in: 33rd Eur. Photovolt. Sol. Energy Conf. Exhib., Amsterdam, The Netherlands, n.d.: pp. 2349–2351. doi:10.4229/EUPVSEC20172017-6BV.2.11.

[16] Fernández, E.F., Muller, M.T., Almonacid, F., Micheli, L., 2019. Soiling Spectral DepositionDetector. USPTO 2019/0312548 A1.

[17] M. Muller, J. Morse, F. Almonacid, E. Fernandez, L. Micheli, Design and Indoor Validation of “DUSST”: A Novel Low-Maintenance Soiling Station, in: 35th Eur. Photovolt. Sol. Energy Conf. Exhib., Bruxelles, Belgium, 2018.

[18] M. Muller, J. Morse, F. Almonacid, E. F. Fernandez and L. Micheli, "Indoor and Outdoor Test Results for "DUSST", a Low-Cost, Low-Maintenance PV Soiling Sensor," 2019 IEEE 46th Photovoltaic Specialists Conference (PVSC), Chicago, IL, USA, 2019, pp. 3277-3280, doi: 10.1109/PVSC40753.2019.8981225.

[19] A. Fernandez-Solas, L. Micheli, M. Muller, F. Almonacid, E. Fernandez, Design, characterization and indoor validation of the optical soiling detector “DUSST”, Solar Energy, Vol. 211, pp 1459-1468, https://doi.org/10.1016/j.solener.2020.10.028

[20] Fernandez, ´ E.F., Muller, M.T., Almonacid, F., Micheli, L., 2019. Soiling Spectral Deposition Detector. USPTO 2019/0312548 A1

[21] L. Micheli, J. Caballero, E Fernandez, G. Smestad, G. Nofuentes, T. Mallick, F. Almonacid, "Correlating photovoltaic soiling losses to waveband and single-value transmittance measurements," Energy, vol. 180, pp. 376–386, 2019.

[22] L. Micheli, E. F. Fernández, M. Muller, G. P. Smestad, and F. Almonacid, "Selection of optimal wavelengths for optical soiling modelling and detection in photovoltaic modules," Sol. Energy Mater. Sol. Cells, vol. 212, August, 2020.

[23] T. Hornung, A. Bachmaier, P. Nitz, A. Gombert, Temperature Dependent Measurement And Simulation Of Fresnel Lenses For Concentrating Photovoltaics, AIP Conference Proceedings 1277, 85 (2010); https://doi.org/10.1063/1.3509239

[24] T. Hornung, M. Neubauerb, A. Gombert, and P. Nitza, Fresnel Lens Concentrator with Improved Thermal Behavior, AIP Conference Proceedings 1407, 66 (2011) https://doi.org/10.1063/1.3658296

[25] M. Muller, B. Marion, S. Kurtz, J. Rodriguez, "Minimizing Variation in Outdoor CPV Power Ratings," CPV7, AIP Conference Proceedings 1407, American Institute of Physics, Melville, NY, 2011.

[26] M. Muller, S. Kurtz, M. Steiner, G. Siefer, Translating outdoor CPV I–V measurements to a CSTC power rating and the associated uncertainty, Prog. Photovolt: vol 23, (11), 2015, https://doi.org/10.1002/pip.2590

[27] Peharz, G., Ferrer Rodrıguez, J., Siefer, G., Bett, A., "Investigations on the Temperature Dependence of CPV Modules Equipped with Triple-Junction Solar Cells," Prog. Photovolt: Res. Appl. 19: pp. 54–60, 2011

[28] J. Cariou, J. Dugas, L. Martin, P. Michel, Refractive-index variations with temperature of PMMA and polycarbonate, Applied Optics Vol. 25, Issue 3, pp. 334-336 (1986), https://doi.org/10.1364/AO.25.000334

[29] A. Cvetkovic, R. Mohedano, O. Gonzalez, P. Zamora, P. Benitez, P. M. Fernandez, A. Ibarreche, M. Hernandez, J. Chaves, and J. Miñano, Performance Modeling of Fresnel-Based CPV Systems: Effects of Deformations under Real Operation Conditions, AIP Conference Proceedings 1407, 74 (2011); https://doi.org/10.1063/1.3658298

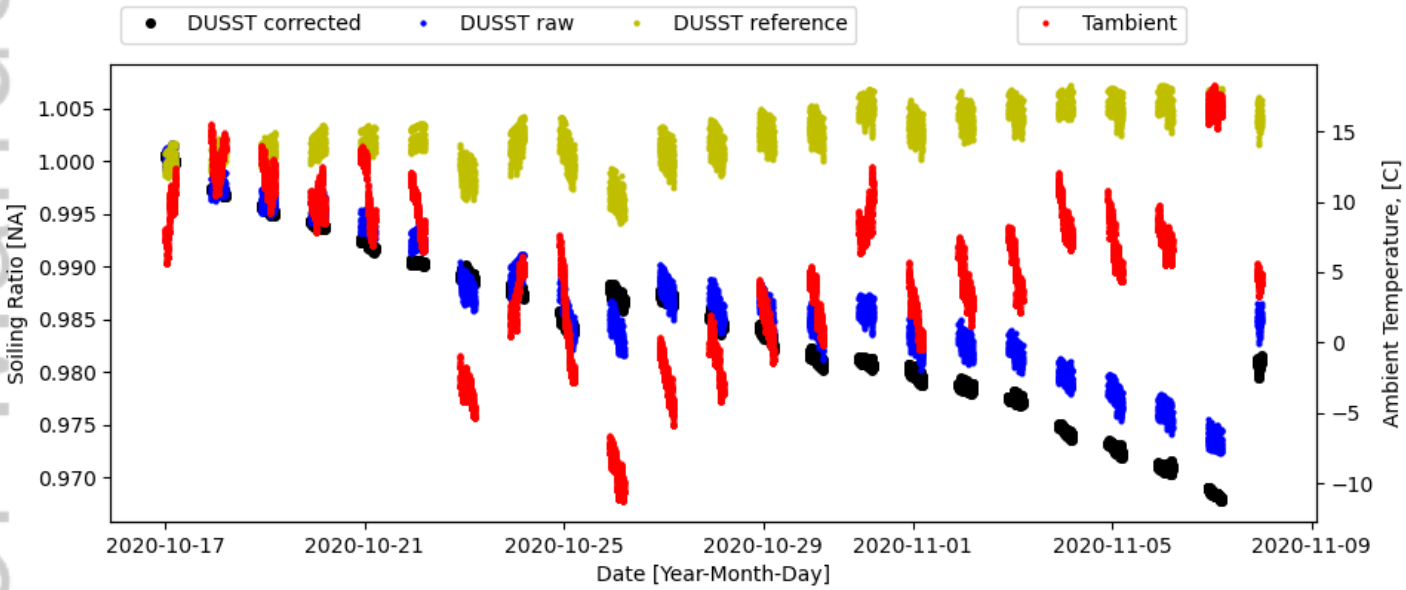

PIP_3415_pip-21-001-File001.png